First-principles phonon calculations of Fe^{4+} impurity in SrTiO$_3$

First-principles phonon calculations of Fe^{4+} impurity in $SrTiO_3$[*]

E Blokhin[1], E A Kotomin[1,2] and J Maier[1]

[1] Max-Planck Institute for Solid State Research, Stuttgart, Germany
[2] Institute of Solid State Physics, University of Latvia, Riga, Latvia

E-mail: e.blokhin@fkf.mpg.de

Abstract

The results of hybrid density functional theory calculations on phonons in $Sr(Fe_xTi_{1-x})O_3$ solid solution within the formalism of a linear combination of atomic orbitals are presented. The phonon density of states (DOS) calculated for 6.25% Fe^{4+} impurities is reported and defect-induced phonon modes are identified. Based on our calculations and group-theoretical analysis, we suggest for the first time an interpretation of experimentally observed Raman- and IR-active modes.

(Some figures may appear in colour only in the online journal)

1. Introduction

The vibrational contribution to the Gibbs free energy is traditionally neglected in first-principles computational studies of point defects and is usually believed to be insignificant. An accurate account of this effect requires the calculation of phonon spectra for low-symmetry systems, which has been an extremely time-consuming task up until now. However, the current capabilities of parallel high-performance computing allow us to perform such calculations. A recent paper [4] serves as a good example of how full phonon calculations and thus taking into account entropy effects at high temperatures make it possible to determine the correct charge state of Ga vacancies in GaAs.

In this paper, we present the results of the first-principles study of phonons for point defects in ABO_3-type perovskites. A case study of Fe^{4+} impurity, substituting a regular Ti^{4+} ion in a $SrTiO_3$ crystal, which serves as a reference model for many similar systems and is relevant for numerous technological applications, is considered.

Defective $Sr(Fe_xTi_{1-x})O_3$ solid solutions are relatively well studied both experimentally (e.g. [5]) and computa-

tionally (e.g. [6, 7]). However, the number of studies on vibrational properties of these systems is very limited. Two Raman measurements [8, 9] and one IR [8] measurement on $Sr(Fe_xTi_{1-x})O_3$ powders have been carried out so far, whereas no attempts have been made to investigate vibrational spectra from first principles. The phonon studies of related defective crystals might also be mentioned, e.g. of oxygen-reduced strontium titanate [10] and iron-doped CoO crystals [11].

2. Computational details

The present study is restricted to the modeling of $Sr(Fe_xTi_{1-x})O_3$ without oxygen vacancies, which is the case for oxidized samples [8]. It is an extension of our previous state-of-the-art studies [12, 13] on phonons in perfect $SrTiO_3$ to the defective case, based on the same computational approach, including also the Hamiltonian and precision settings. The direct frozen-phonon method within a harmonic approximation was adopted. According to this method, each crystallographically independent atom in a defective system was displaced by 0.01 Å from its optimized equilibrium position. The calculation of induced Hellmann–Feynman forces, as well as preliminary geometry optimization, was performed within the formalism of a linear combination of atomic orbitals as implemented in the CRYSTAL09 code [14] using the hybrid exchange–correlation PBE0 functional. This functional was chosen because it gives an accurate description

---

Table 1. Calculated structure relaxation around single Fe^{4+} impurity in $SrTiO_3$.

| Supercell | Iron content (%) | d_{Fe-Fe} (Å) | Distances (Å), displacements in brackets | | E_{relax} (eV) |
			Fe–4 × O planar	Fe–2 × O axial	
80-atom	12.5	7.80	1.90 (−0.06)	2.03 (+0.07)	0.26
80-atom	6.25	11.08	1.88 (−0.08)	2.07 (+0.11)	0.37
160-atom	3.13	13.57	1.88 (−0.08)	2.07 (+0.11)	0.39

of the structural, electronic and vibrational properties of perfect $SrTiO_3$ [13]. Note that for a defect-free $SrTiO_3$, the results given by PBE0 and its effectively screened analog HSE06 are very close [13, 15, 16].

In all defect calculations, a periodic supercell approach was taken, which implies the substitution of a host Ti^{4+} with an Fe^{4+} impurity in the 3D supercell. Each supercell was constructed from a number of primitive cells with the lattice constant of 3.913 Å obtained for perfect $SrTiO_3$ [13].

The iron impurity was described with the basis set (BS) [17], an approach which was successfully used earlier for $Sr(Fe_xTi_{1-x})O_3$ [7]. This BS, along with the BSs for Sr, Ti and O atoms, was optimized according to [18] for the $Sr(Fe_{0.5}Ti_{0.5})O_3$ crystal (the total energy gain due to the optimization is $\sim$0.2 eV per cell). In principle, additional BS optimizations can also be performed for different defect concentrations under investigation. However, as further BS optimization for 25% and 12.5% iron content resulted in a very moderate total energy gain, the same BSs for all the systems with different iron contents were used. Optimization of iron and oxygen BSs for the Fe^{4+} state using the $SrFeO_3$ crystal as the reference model gave a total energy gain of <0.01 eV per cell, and hence was not considered.

3. Results and discussion

Three different concentrations of the Fe^{4+} impurity (12.5%, 6.25% and 3.13%) were considered using 80- and 160-atom supercells [6]. (To model 6.25% and 12.5% iron contents, we used the same 80-atom supercell containing one and two iron atoms, respectively.) High-precision settings are required for phonon calculations in the CRYSTAL09 code. That is why the treatment of even moderate-size supercells at the moment is quite a demanding task. Thus, in this study only the phonons for 6.25% iron content are reported, which, however, fall into the range of defect concentrations studied experimentally [8].

As is well known [6], in the high-spin Fe^{4+} state with $S = 2$ the e_g energy level is occupied by one α-(spin-up) electron, whereas three other α-electrons occupy t_{2g} states. This results in the Jahn–Teller effect and asymmetrical relaxation of the six nearest oxygen atoms surrounding the iron impurity (figure 1). Confirming both general theoretical considerations [19] and the results of the earlier computer modeling [7], the Jahn–Teller displacement pattern of oxygen atoms around the Fe^{4+} impurity was reproduced here (four planar oxygen atoms are displaced towards and two axial oxygen atoms away from the defect).

Both the lattice parameters and internal atomic coordinates were optimized to obtain fully relaxed structures. As
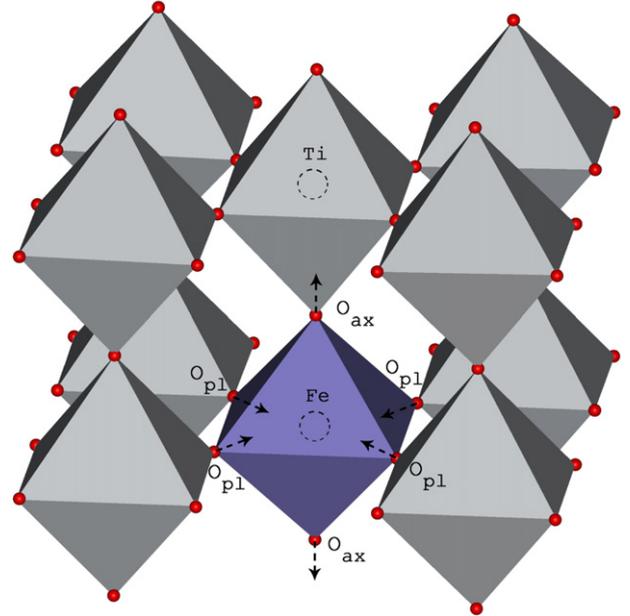

Figure 1. Octahedrally coordinated Fe^{4+} impurity in the $SrTiO_3$ host matrix: the Jahn–Teller effect causes the splitting of surrounding oxygen atoms into two orbits with planar (pl) and axial (ax) O atoms.

a result, the defective crystal structure (starting from cubic symmetry) was reduced to tetragonal symmetry (space group *I*4/*mmm* for 12.5% iron and space group *I*4*mm* for 6.25% and 3.13% iron). The lattice parameter c exceeds the $a = b$ lattice parameters by $\sim$0.05 Å. An additional attempt to model even lower, monoclinic symmetry (space group *Cm*) was performed, but no energy difference from the tetragonal symmetry was found.

The results concerning structural optimization are presented in table 1. It is seen that the decrease of defect concentration leads to an increase of oxygen ion displacements (figure 1), confirming both the theoretical [7] and experimental [8] findings. The increase of distance between periodically distributed Fe impurities (i.e. smaller defect concentrations) results in larger lattice relaxation energies, which, however, saturate at 6.25% concentration. That is, an 80-atom supercell is sufficiently large for defect modeling.

The phonon calculations were performed for such a distorted structure with a fixed spin $S = 2$ (which corresponds to the insulating state), using the 80-atom supercell with tetragonal symmetry. According to this symmetry, group-theoretical analysis [13] predicts that three types of phonon modes are allowed: Raman-active (b_1- and b_2-type), both

Table 2. A comparison of calculated and experimentally observed transverse optical phonon frequencies (cm^{-1}) in SrTiO$_3$ with Fe^{4+} impurity.

Experiment [8] 10% iron	Modeling 6.25% iron
Raman	
170	170 (a$_1$)
250	242 (b$_1$), 243 (a$_1$)
475	469 (e), 478 (e)
545	539 (e), 546 (a$_1$)
690	754 (a$_1$)
IR	
408	421 (e)
445	442 (a$_1$), 459 (e)
645	615 (a$_1$)

IR- and Raman-active (e and a$_1$) and silent (a$_2$). Two acoustic modes (e- and a$_1$-type) close to zero were obtained. It should be noted that the phonons of the defective system were calculated only at the BZ center of a supercell.

The total and partial phonon densities of states (DOSs) were calculated according to [11]. The theoretical DOS is plotted in figure 2 along with the experimental phonon DOS [20] for a perfect crystal and can be compared with the results of IR and Raman measurements [8] on oxidized Sr(Fe$_{0.1}$Ti$_{0.9}$)O$_3$ powders containing only Fe^{4+} impurities. First, the calculated and experimental DOSs reasonably agree, except for the experimental peak at 700 cm^{-1}, which is shifted in calculations down to 800 cm^{-1} (figures 2(a), (b)). In general, a perfect phonon DOS changes insignificantly upon iron doping since Fe and Ti vibrations fall within the same frequency range (see the partial DOS in figure 2(c)). One can see the formation of three groups of Fe-related modes around 150, 300 and 500 cm^{-1}. All the iron-atom vibrational frequencies are of e- or a$_1$-type: the e-type vibrations correspond to the in-plane atomic movements between four inwardly displaced planar oxygen atoms, and the a$_1$-type to out-of-plane movement between two outwardly displaced axial oxygen atoms (figure 1).

For defect-free cubic SrTiO$_3$, no first-order Raman-active frequencies are allowed according to the selection rules. Such frequencies arise however upon material doping. An assignment of the experimentally observed Raman- and IR-active vibrational modes [8] is suggested in table 2. From the analysis of vibrational eigenvectors (similar to that in [13]), we conclude that the first four Raman frequencies here arise due to different types of (Ti, Fe)–O relative vibrations, whereas the last frequency around 690 cm^{-1} is a localized oxygen stretching mode without Ti and Fe ion motion (see the partial DOS in figure 2).

4. Summary

The defective Sr(Fe$_x$Ti$_{1-x}$)O$_3$ systems were considered for several impurity iron concentrations from first principles within a supercell approach using the hybrid exchange–correlation PBE0 functional. The existence of the
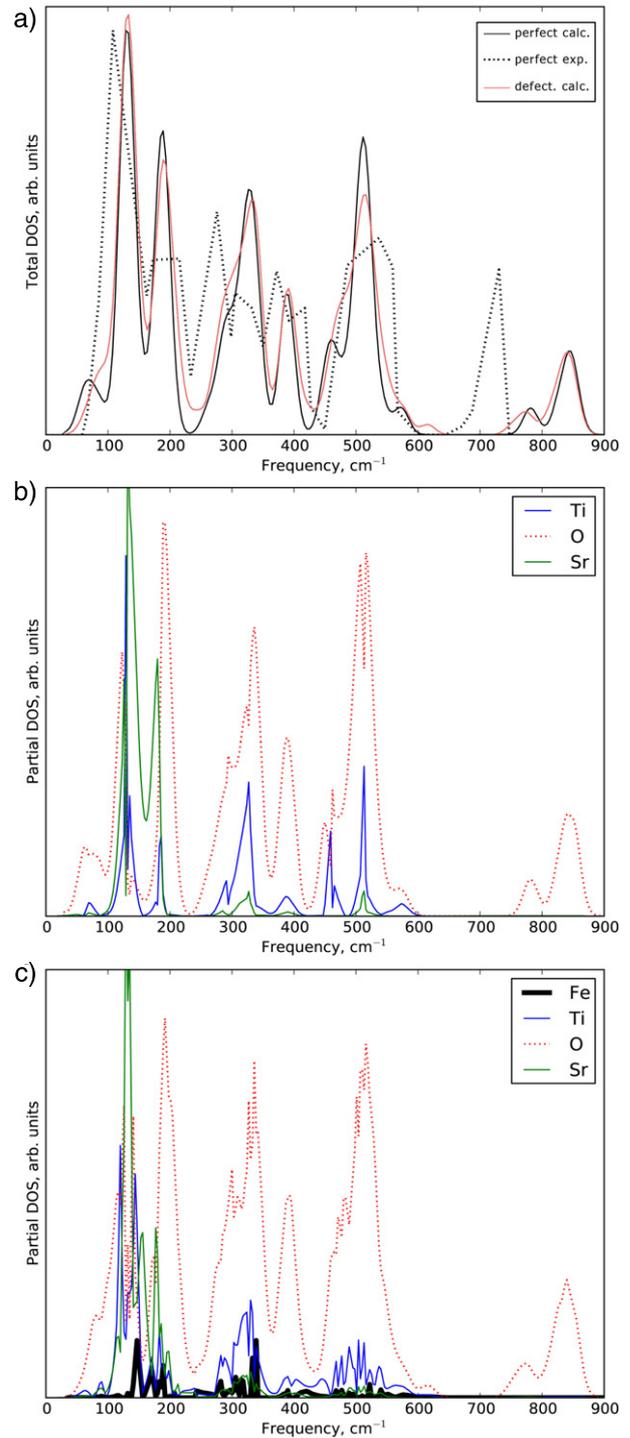

Figure 2. Calculated total (a) and partial ((b) and (c)) phonon DOSs for perfect SrTiO$_3$ (b) and that doped with 6.25% iron (c). The black dotted line in (a) shows the experimental phonon DOS [20]. Partial atomic contributions in (b) and (c) are multiplied for clarity, by a factor of 2 (Sr, Ti, O) and by a factor of 5 (Fe).

Jahn–Teller distortion around the Fe^{4+} impurity, as well as the increase of the surrounding O-atom displacements as iron concentration decreases, was confirmed.

The phonon frequencies were calculated for the first time in defective perovskites at the *ab initio* level. The assignment

of IR and Raman frequency measurements was suggested. In particular, it is shown that Jahn–Teller Fe^{4+} impurity could induce the Raman-active localized oxygen vibrational mode observed around $700\ cm^{-1}$, which does not involve motion of the nearest Fe or Ti ions. Currently, no experimental data exist for the Fe impurity formation energy in perovskites, which could be compared with theoretical Gibbs free energies. This is why the methodology developed in this paper will be used in the forthcoming study of the temperature dependence of oxygen vacancy formation, where such data are available.

Acknowledgments

References

[1] Hizhnyakov V, Tehver I, Boltrushko V and Benedek G 2010 *Eur. Phys. J.* B **75** 187–95
[2] Zipoli F, Bernasconi M and Benedek G 2006 *Phys. Rev.* B **74** 205408
[3] Hizhnyakov V and Benedek G 2005 *Eur. Phys. J.* B **43** 431–8
[4] El-Mellouhi F and Mousseau N 2006 *J. Appl. Phys.* **100** 083521
[5] Merkle R and Maier J 2008 *Angew. Chem. Int. Edn* **47** 3874–94
[6] Evarestov R A, Piskunov S, Kotomin E A and Borstel G 2003 *Phys. Rev.* B **67** 064101
[7] Alexandrov V, Maier J and Evarestov R A 2008 *Phys. Rev.* B **77** 075111
[8] Vrac'ar M, Kuzmin A, Merkle R, Purans J, Kotomin E A, Maier J and Mathon O 2007 *Phys. Rev.* B **76** 174107
[9] Minh N and Phuong D 2011 *J. Exp. Nanosci.* **6** 226–37
[10] Tenne D, Gonenli I, Soukiassian A, Schlom D, Nakhmanson S, Rabe K and Xi X 2007 *Phys. Rev.* B **76** 024303
[11] Wdowik U and Parlinski K 2009 *J. Phys.: Condens. Matter* **21** 125601
[12] Blokhin E, Gryaznov D, Kotomin E, Evarestov R and Maier J 2011 *Int. Ferroelectr.* **123** 18–25
[13] Evarestov R A, Blokhin E, Gryaznov D, Kotomin E and Maier J 2011 *Phys. Rev.* B **83** 134108
[14] Dovesi R *et al* 2009 *CRYSTAL09 User's Manual* (Torino: University of Torino)
[15] El-Mellouhi F, Brothers E N, Lucero M J and Scuseria G E 2011 *Phys. Rev.* B **84** 115122
[16] Wahl R, Vogtenhuber D and Kresse G 2008 *Phys. Rev.* B **78** 104116
[17] Catti M, Valerio G and Dovesi R 1995 *Phys. Rev.* B **51** 7441–50
[18] Evarestov R A, Panin A I, Bandura A V and Losev M V 2008 *J. Phys.: Conf. Ser.* **117** 012015
[19] Dunitz J and Orgel L 1957 *J. Phys. Chem. Solids* **3** 20–9
Bersuker I 2006 *The Jahn–Teller Effect* (Cambridge: Cambridge University Press)
[20] Stirling W 1972 *J. Phys. C: Solid State Phys.* **5** 2711–30